Enhancement of Water Evaporation on Solid Surfaces with Nanoscale Hydrophobic-Hydrophilic Patterns

Rongzheng Wan,[1] Chunlei Wang,[1] Xiaoling Lei,[1] Guoquan Zhou,[2] and Haiping Fang[1,*]
[1]Division of Interfacial Water and Key Laboratory of Interfacial Physics and Technology, Shanghai Institute of Applied Physics, Chinese Academy of Sciences, P.O. Box 800-204, Shanghai 201800, China
[2]School of Sciences, Zhejiang A & F University, Lin'an 311300, P. R. China
(Received 17 April 2015; revised manuscript received 18 August 2015; published 4 November 2015)

Using molecular dynamics simulations, we show that the evaporation of nanoscale water on hydrophobic-hydrophilic patterned surfaces is unexpectedly faster than that on any surfaces with uniform wettability. The key to this phenomenon is that, on the patterned surface, the evaporation rate from the hydrophilic region only slightly decreases due to the correspondingly increased water thickness; meanwhile, a considerable number of water molecules evaporate from the hydrophobic region despite the lack of water film. Most of the evaporated water from the hydrophobic region originates from the hydrophilic region by diffusing across the contact lines. Further analysis shows that the evaporation rate from the hydrophobic region is approximately proportional to the total length of the contact lines.

DOI: 10.1103/PhysRevLett.115.195901 PACS numbers: 68.03.Fg, 66.90.+r, 87.90.+y

The evaporation of water is of fundamental importance in many processes in nature and industry, e.g., transpiration [1], thermoregulation [2], water circulation [3], curing [4], printing [5], and even the survival of bacteria [6]. There have been extensive studies on water evaporation from bulk water surfaces such as the surface of lakes or rivers [3,7,8]. There is usually a tiny and even nanoscale volume of water on various biological and material surfaces, such as those of plant leaves [9], skin [10], or soil [11], a glass surface during papermaking [4], or a surface for printing [5]. The loss of water from those surfaces will cause distinct effects, e.g., plant withering, dehydration, desertification of soil, or improved efficiency for curing and printing. Thus, understanding the evaporation of such tiny or even nanoscale volumes of confined water is essential for many phenomena. Recent work shows that, on various solid surfaces, the evaporation of a thin film of water, i.e., 0.1 μm $-$ 1 mm in thickness, is quite different from the evaporation from bulk water surfaces [12–14]. In 2012, based on molecular dynamics simulation, we found that as a surface changed from hydrophobic to hydrophilic, the evaporation rate *of a small water aggregation (1000 water molecules) supported by the surface* did not simply show a monotonic decrease. Instead, the rate increased to a maximum value and then decreased. The maximum evaporation rate corresponded to the hydrophilic surface, on which water just spread to form a monolayer [15].

Most surfaces in nature are not uniformly hydrophobic or hydrophilic. For example, soil surfaces containing a mixture of components, the back of a desert beetle [16,17], and a leaf surface containing patterns of cells [18,19] all have different wettabilities. It has been found that a patterned structure usually brings about new properties (e.g., the superhydrophobicity resulting from a nanostructure [20–23], or the wetting state change of a droplet on a patterned surface [24–29]), and these properties may lead to potential applications, e.g., self-assembly, self-cleaning, water harvesting, microfluidic pumping or efficient lubrication [16,17,30–33]. We note that many properties of leaves—e.g., photosynthesis [34,35]—have been extensively studied, but no reports have focused on the effect of their surface pattern on water evaporation. Will the patterns enhance or reduce evaporation of a nanoscale volume of water?

In this Letter, we use a nanoscale triangular hydrophobic-hydrophilic pattern as a model to study the evaporation of water on a patterned surface, based on molecular dynamics (MD) simulations. Here, we call a surface hydrophilic if water forms a monolayer on a uniform surface and hydrophobic when water forms a clear droplet, different from the traditional definition based on the contact angle of 90°. We find that the evaporation of a nanoscale volume of water from certain hydrophobic-hydrophilic patterns is faster than that from any surface with uniform wettability, even though the pattern is 43% hydrophobic, and the majority of the hydrophobic surface has no water film. This unexpectedly fast evaporation can be attributed to the slight decrease in the evaporation rate from the hydrophilic region and the considerable number of water molecules that evaporate from the hydrophobic region. Most of the water molecules evaporating from the hydrophobic region come from the hydrophilic region by diffusing across the contact lines, and the evaporation rate on the hydrophobic region is nearly proportional to the total length of the contact lines. Our findings provide a fundamental understanding of water evaporation on nanoscale patterns and offer a guide for controlling the evaporation rate of nanoscale water on solid surfaces.

The solid surface used in this study has dimensions 30 nm $\times$ 30 nm with a planar hexagonal structure of neighboring bond lengths of 0.142 nm. Another solid ceiling with the same dimensions, located 11 nm above the surface, prevents the water molecules from reaching the

other side of the surface through periodic boundary. The patterned surface contains a regular triangular pattern with base line $L_{\text{base}} = 11.4$ nm [Fig. 1(a)]. The hydrophobic region of the pattern is a solid surface without charge, and the atoms in this solid surface have the same Lennard-Jones parameters as the carbon in graphite [36,37]. Graphite is usually regarded as hydrophobic [38], and simulations show that water has a contact angle near 50° [Fig. 1(b)] on the uniform solid surface without charges. The same solid surface with charges is the hydrophilic region, and water just spreads to form a monolayer on this hydrophilic surface. As shown in Fig. 1(c), the hydrophilic region has the same geometry as the solid substrate used in our previous work [15]; positive and negative charges of the same magnitude q were assigned to the atoms at a distance

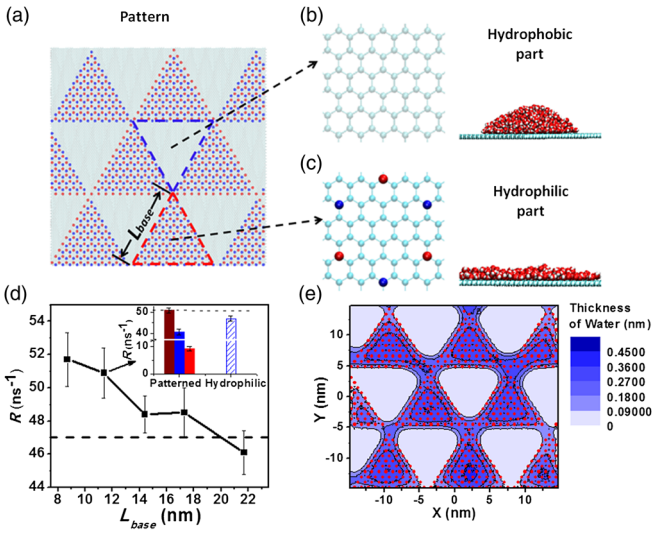

FIG. 1 (color online). Water evaporation on a patterned surface. (a) Geometry of the patterned surface. The red and blue dashed regular triangles outline the hydrophilic and hydrophobic patterns, respectively. The base line of the regular triangle (L_{base}) is 11.4 nm. (b), (c) Detailed geometry of the hydrophobic and hydrophilic parts of the pattern, respectively. The blue and red spheres represent atoms with positive and negative charges of 0.4 e, respectively, while the gray spheres represent neutral atoms. The snapshots on the right show the water formation on the uniformly hydrophobic and hydrophilic surfaces, these surfaces have the same geometries as the hydrophobic and hydrophilic parts of the pattern. (d) The evaporation rate R of 10 505 water molecules on patterned surfaces with different L_{base}, together with the evaporation rate of the same amount of water on the maximal-evaporation uniform surface (dashed line). Inlet shows the evaporation rate R of 10 505 water molecules on a patterned surface with $L_{\text{base}} = 11.4$ nm and the maximal-evaporation uniform surface. The brown, blue, and red solid columns represent the total evaporation rate R_{total}, the evaporation rate $R_{\text{hydrophilic}}$ from the hydrophilic region, and the evaporation rate $R_{\text{hydrophobic}}$ from the hydrophobic region on the patterned surface, respectively. The blue open column denotes the evaporation rate from the maximal-evaporation uniform surface. (e) Contour map of the water thickness on the patterned surface. The red points represent the positions of the charges which outline the hydrophilic region.

of 0.568 nm (twice the diagonal of the hexagon). Here, $q = 0.4\,e$, which corresponds to the maximum evaporation rate on such a substrate as shown in our previous work [15]. Overall, the patterned surface contains 550 positive charges and 550 negative charges; thus, it was neutral. The uniformly hydrophilic surface used for comparison has the same charge geometry as that shown in Fig. 1(c). We also used a solid surface containing a hydrophilic stripe to study the evaporation of water near the pattern boundaries. The stripe pattern has dimensions 32 nm × 5 nm, with a hydrophilic stripe 8 nm in width. The hydrophilic stripe has the same geometry as that shown in Fig. 1(c).

Initially, 10 505 water molecules in a cubic shape, with dimensions 28 nm × 28 nm × 0.4 nm, were deposited 0.5 nm above the patterned and hydrophilic surface, respectively. An accelerating region was applied from 4 nm to 5.5 nm above the surface. When a water molecule runs into the accelerating region, an upward force of 1.0 kcal × mol^{-1} Å^{-1} [force vector (0, 0, 1)] was applied to the oxygen atom to prevent the water molecule from going back to the lower surface. This nonequilibrium condition is equivalent to the setting of other literature in which evaporated molecules run into an infinite vacuum [39]. The number of water molecules entering the accelerating region from the surface per nanosecond is defined as the evaporation rate R, and the evaporation rate per nm^2 on the surface is defined as the evaporation flux J.

MD simulations, which have been widely used to study water dynamics in nanoscale systems [40–52], were performed in a box with initial size 30 nm × 30 nm × 13 nm. The calculation, using NAMD 2.9 [53], had a time step of 2 fs. Periodic boundary conditions were applied to all three coordinates x, y, z. The Lennard-Jones parameters of the atoms in the solid surface were $\varepsilon = 0.07$ kcal mol^{-1} and $\sigma = 0.4$ nm [36,37], and the rigid TIP3P [54] water model was used (simulation results with SPC/E water model can be seen in PS1 of Supplemental Material [55]). Particle mesh Ewald (PME) integration was used to treat the long-range electrostatic interactions. Berendsen temperature coupling [56] was applied every 20 steps to keep the system at 300 K (simulation results at 320 K can also be seen in PS2 of Supplemental Material [55]). For the surface with a stripe pattern, the simulation box had an initial size of 32 nm × 5 nm × 13 nm; the other simulation parameters were the same. The trajectories of the coordinate and velocity were collected every 1 ps. The duration time of the evaporation could not be very long in order to keep the number of water molecules on the surface close to the initial value. Thus, for each surface, after an equilibrium MD simulation for 5 ns, we constructed tens independent systems. The accelerating region was applied in each system and data were collected for 10 ns. All the data were averaged from these ten systems.

We showed in our previous study [15] that, on a surface with uniform wettability, the fastest evaporation occurs on the hydrophilic surface on which the water just spread to form a monolayer. We call this surface the

maximal-evaporation uniform surface. The average evaporation flux (evaporation rate per nm^2) on this maximal-evaporation uniform surface is denoted by J_{max}. In the present simulation, $J_{max} = 0.0523 \pm 0.0014$ ns^{-1} nm^{-2}. Since only 57% of the patterned surface is the hydrophilic region, an intuitive estimation suggests that the total evaporation rate R_{total} on the patterned surface would be much smaller than $J_{max} \times S_{total}$, where $S_{total} = 900$ nm^2 is the total area of the surface. However, to our surprise, calculations show that R_{total} on the patterned surface has an average value of 50.9 ± 1.4 ns^{-1}, which is larger than R_{total} on the maximal-evaporation uniform surface [$J_{max} \times S_{total} = 0.0523$ ns^{-1} $nm^{-2} \times 900$ $nm^2 = 47.1 \pm 1.3$ ns^{-1}; see Fig. 1(d)]. This suggests that the pattern enhances the evaporation of nanoscale water.

To understand this unexpectedly fast evaporation rate, we first examine the water state on the patterned surface. As shown in Fig. 1(e), most water molecules are confined to the hydrophilic region of the surface, and they separate into several films surrounded by the hydrophobic region. The total evaporation rate from the hydrophilic region, $R_{hydrophilic}$, is 40.7 ± 1.3 ns^{-1}. Interestingly, this value is considerably larger than $J_{max} \times S_{hydrophilic} = 0.0523$ ns^{-1} $nm^{-2} \times 510$ $nm^2 = 26.7$ ns^{-1}; here, $S_{hydrophilic}$ is the area of the hydrophilic region on the patterned surface. This is because the average evaporation flux $J = 0.0798 \pm 0.0025$ ns^{-1} nm^{-2} on the hydrophilic region of the patterned surface is larger than J_{max}. Careful examination shows that the average thickness of water on the hydrophilic region of the patterned surface is ~0.50 nm, which is larger than the average thickness of water on the maximal-evaporation uniform surface (~0.35 nm). It seems that the correspondingly increased water thickness enhances the evaporation flux from the hydrophilic region, and partly compensates for the effect of the decreased hydrophilic area. Meanwhile, there is a $R_{hydrophobic}$ of 10.2 ± 1.0 ns^{-1} from the hydrophobic region. Although the majority of hydrophobic parts have no water film, a considerable number of water molecules diffuse from the hydrophilic region across the contact lines and then evaporate. Finally, $R_{total} = R_{hydrophilic} + R_{hydrophobic}$ on the patterned surface reaches 50.9 ± 1.4 ns^{-1} and exceeds R_{total} on the maximal-evaporation uniform surface (47.1 ± 1.3 ns^{-1}) with the same surface area. (The detail of counting $R_{hydrophilic}$ and $R_{hydrophobic}$ can be seen in PS3 of Supplemental Material [55]).

We further examine the effect of water thickness on evaporation by analyzing the evaporation of different amounts of water on a surface containing an 8 nm wide hydrophilic stripe [Fig. 2(a)]. The hydrophilic stripe has the same wettability as the maximal-evaporation uniform surface. Initially, there are 398, 547, 697, 850, and 1000 water molecules on the surface. After equilibrating for 5 ns, the water molecules are confined to the hydrophilic stripe, and the average thicknesses of the water films on the hydrophilic region are 0.29, 0.40, 0.50, 0.61, and 0.72 nm, respectively. As shown in Fig. 2(b), the evaporation flux J from hydrophilic region first increases sharply with water thickness, then the variation in J flattens when the water thickness reaches 0.50 nm. This can be attributed to the average total interaction energy E_{total} for each outmost water molecule in the water film, which acts as the energy barrier that prevents evaporation of the water molecule. Here, E_{total} is sum of the water-surface interaction energy $E_{water\text{-}surface}$ and the water-water interaction energy $E_{water\text{-}water}$. As shown in Fig. 2(c), $E_{water\text{-}water}$ only slightly strengthens as the water thickness increases, while $E_{water\text{-}surface}$ significantly weakens and becomes negligible when the water thickness is equal to or larger than 0.50 nm. Clearly, the variation of E_{total} is mainly caused by the change in $E_{water\text{-}surface}$. $E_{water\text{-}surface}$ is mainly provided by the electrical interaction between the outmost water molecules and the charges assigned on the hydrophilic region of the substrate, which is decided by the distance between the outmost water molecule and the surface, i.e., water thickness. As the water thickness increases, the weakening of E_{total} facilitates the evaporation of the outmost water molecules in the water film and enhances the evaporation flux from the hydrophilic region before the water thickness becomes too large. When the water thickness is large enough (greater than 0.50 nm in our simulation), the influence of the water thickness on E_{total} becomes negligible, and the evaporation flux seems independent of the water thickness.

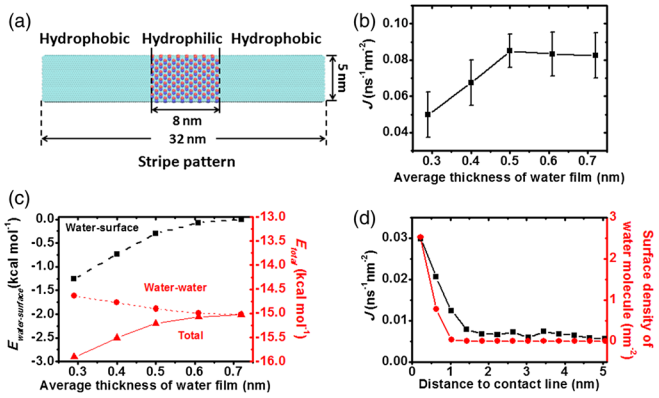

FIG. 2 (color online). Water evaporation on striped patterns. (a) Surface geometry with striped pattern. The hydrophilic stripe has a width of 8 nm. (b) Evaporation flux J from the hydrophilic region vs the average thickness of water on the hydrophilic region of the striped pattern. (c) Average interaction energy for each outmost water molecules in the water film vs the average thickness of water film. The red triangles, black squares, and red circles represent the average total interaction energy E_{total}, the average interaction energy $E_{water\text{-}surface}$ between water and the solid surface, and the average interaction energy $E_{water\text{-}water}$ between water molecules, respectively. (d) Evaporation flux J and the surface density of water on the hydrophobic region vs the distance to the contact lines. The black squares and the red circles represent the evaporation flux J and the surface density of water molecules, respectively.

Now, we further analyze the evaporation from the hydrophobic region by calculating the water evaporation on the stripe pattern. The initial number of water molecules on the stripe pattern is 547. As shown in Fig. 2(d), the evaporation flux from the hydrophobic region decreases sharply as the distance from the contact lines increases, and the evaporation flux remains at a very low level when the distance is larger than 2 nm. This can be attributed to the distribution of the water density on the hydrophobic region, as shown in Fig. 2(d). The water density decreases sharply as the distance to the contact lines increases. There is almost no water film on the hydrophobic region, and most of the evaporated water molecules originate from the hydrophilic region by diffusing across the contact lines. Since the evaporation rate on the hydrophobic region mainly comes from the area near the contact lines (which coincide with the pattern boundaries for nanoscale water evaporation), patterns with different boundary lengths may have different effects on water evaporation.

Here, we calculate the evaporation of the same amount of water on patterns with different sizes. These surfaces both have regular triangular hydrophobic-hydrophilic patterns, similar to Fig. 1(a), but with a different length of the base line L_{base}. Figure 3(a) shows snapshots of 10 505 water molecules on the regular triangular patterns, with $L_{\mathrm{base}} = 8.7$, 14.4, 17.3, and 21.7 nm. The areas of these patterns are 55%–60% hydrophilic. We can see that most of the water molecules are confined to the hydrophilic region, and that the contact lines of the water film almost coincide with the pattern boundaries. The average evaporation rate decreases monotonically as L_{base} increases [Fig. 1(d)]. Actually, L_{boundary} decreases as L_{base} increases. Figure 3(b) shows the evaporation rate on patterned surfaces vs L_{boundary}; the dashed line is the linear fit of the evaporation rate $R = 42.0 + 0.03 \times L_{\mathrm{boundary}}$. Since all the hydrophilic regions on these patterns are quite close in area (500–540 nm^2), $R_{\mathrm{hydrophilic}}$ on these patterns are almost consistently 42.0 ns^{-1}. Thus, the evaporation rate from the hydrophobic region can be written as $R_{\mathrm{hydrophobic}} \approx 0.03 \times L_{\mathrm{boundary}}$. This indicates that the evaporation rate on the hydrophobic region is approximately proportional to the total length of the pattern boundaries, which is nearly equal to the total length of the contact lines. We note that, in Fig. 3(b), the evaporation rate on the pattern with $L_{\mathrm{base}} = 21.7$ nm is below that on the maximal-evaporation uniform surface (dashed line). This means that the large-size pattern reduces the evaporation of water. This inspires us that it is possible to control the evaporation rate of nanoscale water on solid surfaces by using hydrophobic-hydrophilic patterns of different sizes and boundary lengths. A nanoscale pattern with longer boundaries may obviously enhance the evaporation rate of water, and a large-size pattern with shorter boundaries may help conserve nanoscale water on a surface.

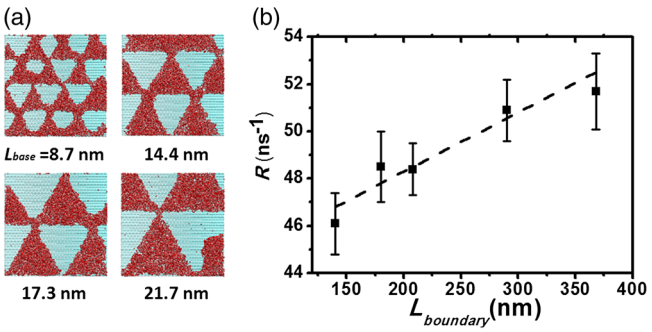

FIG. 3 (color online). Water evaporation from patterns with different sizes. (a) Snapshot of 10 505 water molecules on surfaces containing a regular triangular pattern. The base line $L_{\mathrm{base}} = 8.7$, 14.4, 17.3, and 21.7 nm. The red points represent the water molecules. (b) The evaporation rate R of 10 505 water molecules on the patterned surfaces vs the total length of the boundaries L_{boundary} together with the linear fit (dashed line).

In summary, using MD simulations, we found that the evaporation of nanoscale water on hydrophobic-hydrophilic patterned surfaces is faster than that on surfaces with uniform wettability. This intensive water evaporation is due to the slight decrease in evaporation rate from the hydrophilic region and the considerable evaporation rate from the hydrophobic region. On the hydrophilic region, the evaporation flux increases sharply with water thickness until the thickness reaches 0.50 nm. Thus, for nanoscale water, although the patterned surface is only 57% hydrophilic, the correspondingly increased water thickness results in a slight decrease in water evaporation. Meanwhile, water molecules do evaporate from the hydrophobic region, even though the majority of the region has no water film. This is mainly due to diffusion out of the hydrophilic region across the contact lines that coincide with pattern boundaries. Our simulations show that the evaporation rate in the hydrophobic region is almost proportional to the total length of the contact lines. We note that the water contact lines affect many of the behaviors of nanoscale water, e.g., the contact angle of water [57,58]. For the evaporation of water on nanoscale patterns, the length of the contact lines also plays an important role. Our findings provide a fundamental understanding of water evaporation on nanoscale-patterned surfaces, offers insights into understanding the transpiration on biological surfaces and also leads to potential applications for regulating the evaporation of nanoscale water on a solid surface.

We thank Yi Gao, Guosheng Shi, Wenpeng Qi, and Jian Liu for their constructive suggestions. This work was supported by NNSFC (Grants No. 11290164, No. 11204341, No. 11474299), the Key Research Program of CAS (KJZD-EW-M03), the Deepcomp7000 and ScGrid of Supercomputing Center, Computer Network Information Center of Chinese Academy of Sciences, and the Shanghai Supercomputer Center of China.

*fanghaiping@sinap.ac.cn

[1] R. Leuning, F. M. Kelliher, D. G. G. Depury, and E. D. Schulze, Plant Cell Environ. **18**, 1183 (1995).
[2] D. Fiala, K. J. Lomas, and M. Stohrer, J. Appl. Physiol. **87**, 1957 (1999).
[3] M. A. Kohler and L. H. Parmele, Water Resour. Res. **3**, 997 (1967).
[4] W. Shen, N. Brack, H. Ly, I. H. Parker, P. J. Pigram, and J. Liesegang, Colloid Surf. A-Physicochem. Eng. Asp. **176**, 129 (2001).
[5] J. Park and J. Moon, Langmuir **22**, 3506 (2006).
[6] X. J. Xie, Y. G. Li, T. Zhang, and H. H. P. Fang, Appl. Microbiol. Biotechnol. **73**, 703 (2006).
[7] I. W. Eames, N. J. Marr, and H. Sabir, Int. J. Heat Mass Transfer **40**, 2963 (1997).
[8] V. Ramanathan, P. J. Crutzen, J. T. Kiehl, and D. Rosenfeld, Science **294**, 2119 (2001).
[9] R. L. Jones, Physiol Plant. **10**, 281 (1957).
[10] R. O. Potts and M. L. Francoeur, Proc. Natl. Acad. Sci. U.S.A. **87**, 3871 (1990).
[11] G. Zarei, M. Homaee, A. M. Liaghat, and A. H. Hoorfar, J. Hydrol. **380**, 356 (2010).
[12] M. Elbaum and S. G. Lipson, Phys. Rev. Lett. **72**, 3562 (1994).
[13] D. H. Shin, S. H. Lee, J.-Y. Jung, and J. Y. Yoo, Microelectron. Eng. **86**, 1350 (2009).
[14] M. Lee, D. Lee, N. Jung, M. Yun, C. Yim, and S. Jeon, Appl. Phys. Lett. **98**, 013107 (2011).
[15] S. Wang, Y. Tu, R. Wan, and H. Fang, J. Phys. Chem. B **116**, 13863 (2012).
[16] X. Yao, Y. Song, and L. Jiang, Adv. Mater. **23**, 719 (2011).
[17] A. R. Parker and C. R. Lawrence, Nature (London) **414**, 33 (2001).
[18] M. E. Byrne, R. Barley, M. Curtis, J. M. Arroyo, M. Dunham, A. Hudson, and R. A. Martienssen, Nature (London) **408**, 967 (2000).
[19] H. Wang, N. Ngwenyama, Y. Liu, J. C. Walker, and S. Zhang, Plant Cell **19**, 63 (2007).
[20] L. Feng, S. H. Li, H. J. Li, J. Zhai, Y. L. Song, L. Jiang, and D. B. Zhu, Angew. Chem., Int. Ed. Engl. **41**, 1221 (2002).
[21] E. Martines, K. Seunarine, H. Morgan, N. Gadegaard, C. D. W. Wilkinson, and M. O. Riehle, Nano Lett. **5**, 2097 (2005).
[22] C. Yang, U. Tartaglino, and B. N. J. Persson, Phys. Rev. Lett. **97**, 116103 (2006).
[23] X. D. Zhao, H. M. Fan, X. Y. Liu, H. H. Pan, and H. Y. Xu, Langmuir **27**, 3224 (2011).
[24] Y. C. Jung and B. Bhushan, Scr. Mater. **57**, 1057 (2007).
[25] J. B. Wu, M. Y. Zhang, X. Wang, S. B. Li, and W. J. Wen, Langmuir **27**, 5705 (2011).
[26] J. H. Wang, D. Bratko, and A. Luzar, Proc. Natl. Acad. Sci. U.S.A. **108**, 6374 (2011).
[27] R. Godawat, S. N. Jamadagni, and S. Garde, Proc. Natl. Acad. Sci. U.S.A. **106**, 15119 (2009).
[28] T. A. Ho, D. V. Papavassiliou, L. L. Lee, and A. Striolo, Proc. Natl. Acad. Sci. U.S.A. **108**, 16170 (2011).
[29] N. Giovambattista, P. G. Debenedetti, and P. J. Rossky, Proc. Natl. Acad. Sci. U.S.A. **106**, 15181 (2009).
[30] L. Zhai, M. C. Berg, F. C. Cebeci, Y. Kim, J. M. Milwid, M. F. Rubner, and R. E. Cohen, Nano Lett. **6**, 1213 (2006).
[31] D. M. Huang, C. Cottin-Bizonne, C. Ybert, and L. Bocquet, Phys. Rev. Lett. **101**, 064503 (2008).
[32] M. Suttipong, B. P. Grady, and A. Striolo, Phys. Chem. Chem. Phys. **16**, 16388 (2014).
[33] J. Seror, L. Zhu, R. Goldberg, A. J. Day, and J. Klein, Nat. Commun. **6**, 6497 (2015).
[34] V. K. Yachandra, K. Sauer, and M. P. Klein, Chem. Rev. **96**, 2927 (1996).
[35] A. Zouni, H. T. Witt, J. Kern, P. Fromme, N. Krauss, W. Saenger, and P. Orth, Nature (London) **409**, 739 (2001).
[36] D. Lu, Y. Li, U. Ravaioli, and K. Schulten, J. Phys. Chem. B **109**, 11461 (2005).
[37] J. Goldsmith and C. C. Martens, J. Phys. Chem. Lett. **1**, 528 (2010).
[38] D. Li, M. B. Muller, S. Gilje, R. B. Kaner, and G. G. Wallace, Nat. Nanotechnol. **3**, 101 (2008).
[39] V. Zhakhovskii and S. Anisimov, J. Exp. Theor. Phys. **84**, 734 (1997).
[40] A. V. Raghunathan and N. R. Aluru, Phys. Rev. Lett. **97**, 024501 (2006).
[41] B. Y. Wang and P. Kral, Phys. Rev. Lett. **101**, 046103 (2008).
[42] Y. von Hansen, S. Gekle, and R. R. Netz, Phys. Rev. Lett. **111**, 118103 (2013).
[43] I. Kosztin and K. Schulten, Phys. Rev. Lett. **93**, 238102 (2004).
[44] G. Hummer, J. C. Rasaiah, and J. P. Noworyta, Nature (London) **414**, 188 (2001).
[45] B. L. de Groot and H. Grubmuller, Science **294**, 2353 (2001).
[46] R. H. Zhou, X. H. Huang, C. J. Margulis, and B. J. Berne, Science **305**, 1605 (2004).
[47] N. Giovambattista, P. J. Rossky, and P. G. Debenedetti, Phys. Rev. Lett. **102**, 050603 (2009).
[48] E. G. Strekalova, J. Y. Luo, H. E. Stanley, G. Franzese, and S. V. Buldyrev, Phys. Rev. Lett. **109**, 105701 (2012).
[49] C. L. Wang, H. J. Lu, Z. G. Wang, P. Xiu, B. Zhou, G. H. Zuo, R. Z. Wan, J. Z. Hu, and H. P. Fang, Phys. Rev. Lett. **103**, 137801 (2009).
[50] L. Zhao, C. L. Wang, J. Liu, B. H. Wen, Y. S. Tu, Z. W. Wang, and H. P. Fang, Phys. Rev. Lett. **112**, 078301 (2014).
[51] T. Koishi *et al.*, Phys. Rev. Lett. **93**, 185701 (2004).
[52] C. Q. Zhu, H. Li, Y. F. Huang, X. C. Zeng, and S. Meng, Phys. Rev. Lett. **110**, 126101 (2013).
[53] J. C. Phillips *et al.*, J. Comput. Chem. **26**, 1781 (2005).
[54] W. L. Jorgensen, J. Chandrasekhar, J. D. Madura, R. W. Impey, and M. L. Klein, J. Chem. Phys. **79**, 926 (1983).
[55] See Supplemental Material at http://link.aps.org/supplemental/10.1103/PhysRevLett.115.195901 for more detailed simulation data.
[56] H. J. C. Berendsen, J. P. M. Postma, W. F. v. Gunsteren, A. DiNola, and J. R. Haak, J. Chem. Phys. **81**, 3684 (1984).
[57] A. Checco, P. Guenoun, and J. Daillant, Phys. Rev. Lett. **91**, 186101 (2003).
[58] H. K. Guo and H. P. Fang, Chin. Phys. Lett. **22**, 787 (2005).